Electronic Supplementary Information

Spectroscopic Insight on Impact of Environment on Natural Photoprotectants

Abigail L. Whittock,[a,b] Xuefei Ding,[c] Xavier E. Ramirez Barker,[c] Nazia Auckloo,[a,d] Rebecca A. Sellers,[a] Jack M. Woolley,[c] Krishnan Tamareselvy,[e] Marine Vincendet,[f] Christophe Corre,[a,d] Emma Pickwell-MacPherson[c] and Vasilios G. Stavros*[a,g]

[a]Department of Chemistry, University of Warwick, Coventry, CV4 7AL, United Kingdom; [b]Analytical Science Centre for Doctoral Training, University of Warwick, Coventry, CV47AL, United Kingdom; [c]Department of Physics, University of Warwick, Coventry, CV4 7AL, United Kingdom; [d]Warwick Integrative Synthetic Biology Centre and School of Life Sciences, University of Warwick, Coventry CV4 7AL, United Kingdom. [e]Lubrizol Advanced Materials Inc., 377 Hoes Lane, Suite 210, Piscataway, New Jersey-08854, United States of America. [f]Lubrizol Life Science Beauty, Calle Isaac Peral, 17 Pol. Ind. Camí Ral, 08850 Barcelona, Spain; [g]School of Chemistry, University of Birmingham, Edgbaston, Birmingham, B15 2TT, United Kingdom.

* Corresponding author: v.stavros@warwick.ac.uk

Experimental Procedure Details

Extraction and characterisation

5 g batches of dried Palmaria palmata (P. palmata) flakes (The Cornish Seaweed Company) were left to macerate overnight at 4ºC in a mixture of 25:75 HPLC-grade methanol to HPLC-grade water. The next day, the sample was sonicated for 5 cycles of 45 s with 1 minute intervals, followed by centrifugation and recovery of the supernatant which was afterwards dried using a centrifugal evaporator to yield ~1 g of crude extract for each initial 5 g batch of dried P. palmata. The consistency of the crude extract was a thick brown oil which partly crystalised.
Part of the crude extract was resuspended in HPLC-grade water and filtered through 0.25 μm filters in preparation for ultra high performance liquid chromatography – high resolution mass spectrometry (UHPLC-HRMS) analysis. The analysis was performed with a 2 μL sample injection through a reverse phase column (Zorbax Eclipse Plus C18, size 2.1 x 100 mm, particle size 1.8 μm) connected to a Dionex 3000RS UHPLC coupled to Bruker Ultra High Resolution (UHR) Q-TOP MS MaXis II mass spectrometer using Electrospray Ionization (ESI) in positive mode with 10 mM sodium formate injected at the start of each run for internal calibration. A m/z range of 50-2500 was used. Column elution was done with the following gradient: 0 to 25 % solvent B for 30 mins (solvent A = 0.1% formic acid in water and solvent B = 0.1% formic acid in acetonitrile). The base peak chromatogram (BPC) and extracted ion chromatograms (EIC) are given in Figure S1. The following mycosporine-like amino acids (MAAs) were identified in the sample based on the accurate m/z values being consistent with their molecular formula, these are reported below and presented in Figures S2-9. The assignment was also guided by previous data reporting on the identification of MAAs in P. palmata.[1-3]

Mycosporine-like amino acids (MAAs) identified by UHPLC-HRMS analysis:

Palythine: HRMS (ESI-TOF) m/z: [M+H]+ Calculated for $C_{10}H_{17}N_2O_5^+$ 245.1132; Found 245.1133; error 0.4 ppm

Mycosporine-glycine: HRMS (ESI-TOF) m/z: [M+H]+ Calculated for $C_{10}H_{15}N_1O_6^+$ 246.0972; Found 246.0971; error 0.4 ppm

Usujirene: HRMS (ESI-TOF) m/z: [M+H]+ Calculated for $C_{13}H_{21}N_2O_5^+$ 285.1445; Found 285.1448; error 1.1 ppm

Palythene: HRMS (ESI-TOF) m/z: [M+H]+ Calculated for $C_{13}H_{21}N_2O_5^+$ 285.1445; Found 285.1449; error 1.4 ppm

Asterina-330: HRMS (ESI-TOF) m/z: [M+H]+ Calculated for $C_{12}H_{21}N_2O_6^+$ 289.1394; Found 289.1395; error 0.3 ppm

Palythinol: HRMS (ESI-TOF) m/z: [M+H]+ Calculated for $C_{13}H_{23}N_2O_6^+$ 303.1551; Found 303.1550; error 0.3 ppm

Shinorine: HRMS (ESI-TOF) m/z: [M+H]+ Calculated for $C_{13}H_{21}N_2O_8^+$ 333.1292; Found 333.1294; error 0.6 ppm

Porphyra-334: HRMS (ESI-TOF) m/z: [M+H]+ Calculated for $C_{14}H_{23}N_2O_8^+$ 347.1449; Found
347.1449; error 0.0 ppm

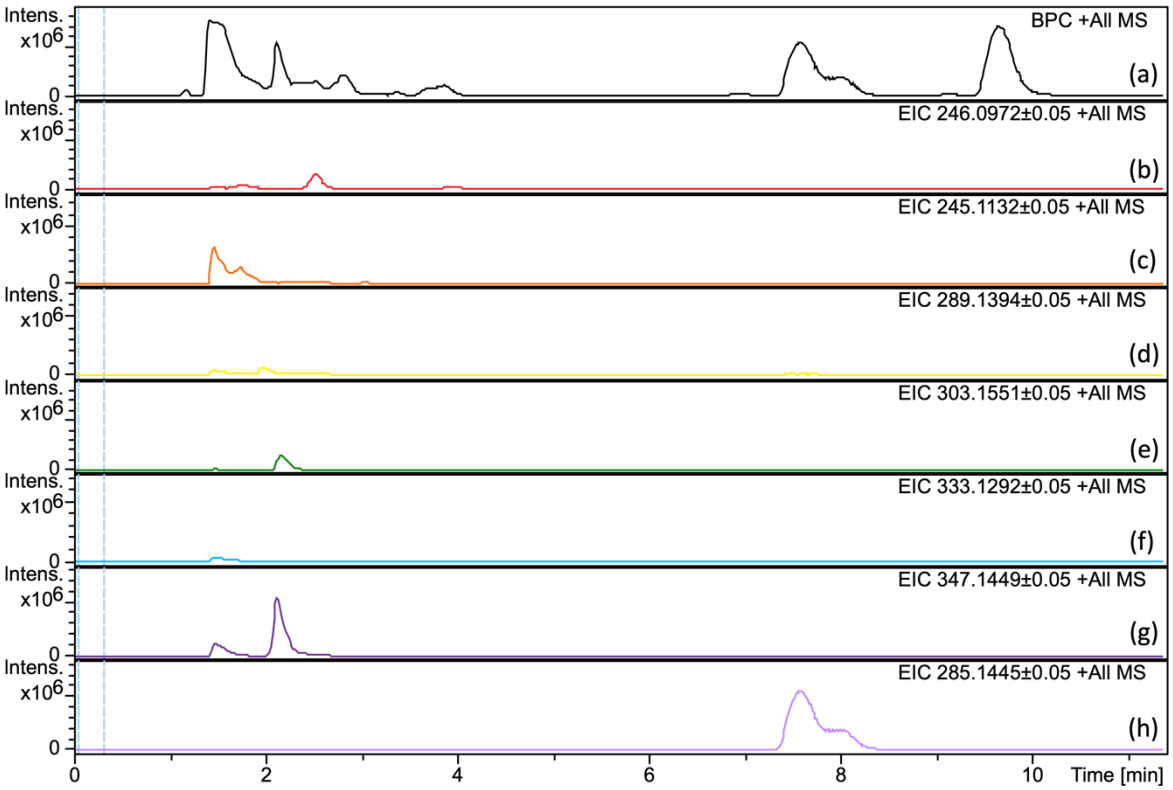

Figure S1. (a) BPC of the crude extract. EIC for (b) mycosporine-glycine (c) palythine, (d) asterina330, (e) palythinol, (f) shinorine, (g) porphyra-334 and (h) usujirene/palythene.

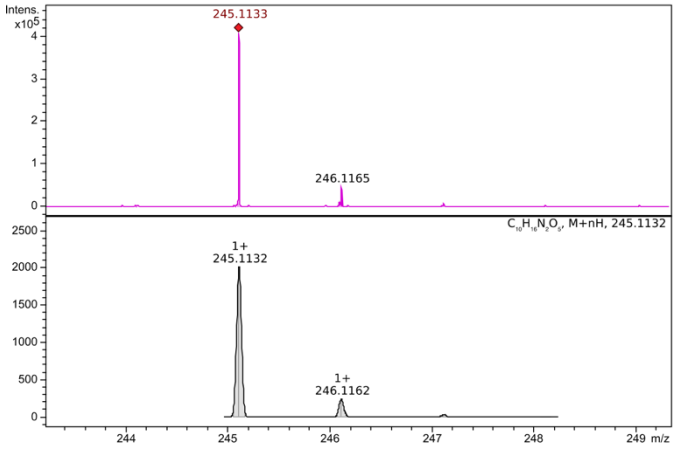

Figure S2. Comparison of the measured (pink) and simulated (black) $[M+H]^+$ mass spectra for palythine.

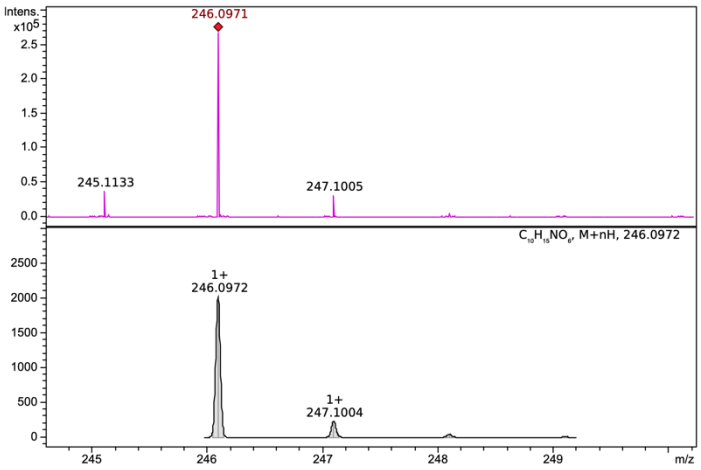

Figure S3. Comparison of the measured (pink) and simulated (black) $[M+H]^+$ mass spectra for mycosporine-glycine.

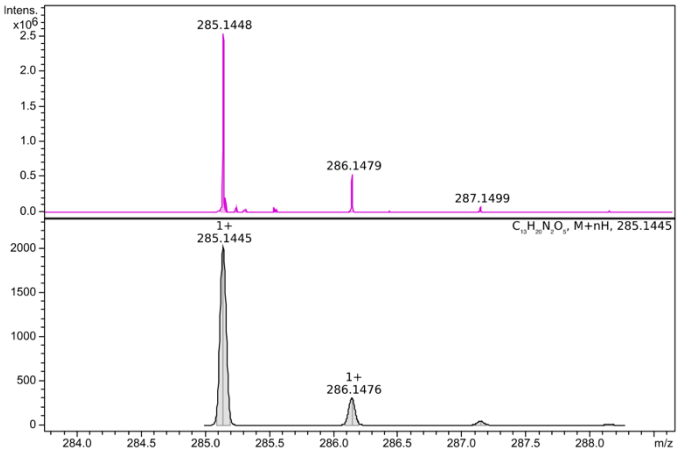

Figure S4. Comparison of the measured (pink) and simulated (black) $[M+H]^+$ mass spectra for usujirene.

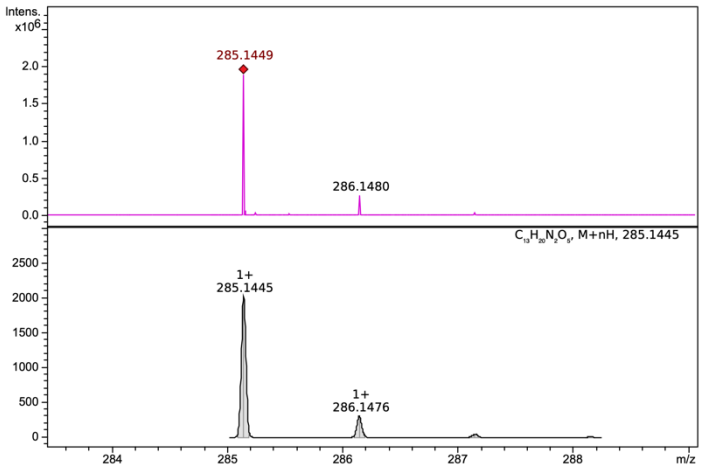

Figure S5. Comparison of the measured (pink) and simulated (black) $[M+H]^+$ mass spectra for palythene.

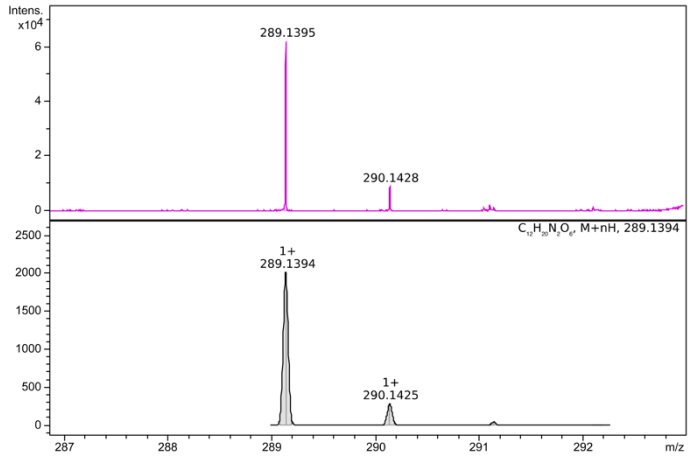

Figure S6. Comparison of the measured (pink) and simulated (black) $[M+H]^+$ mass spectra for asterina-330.

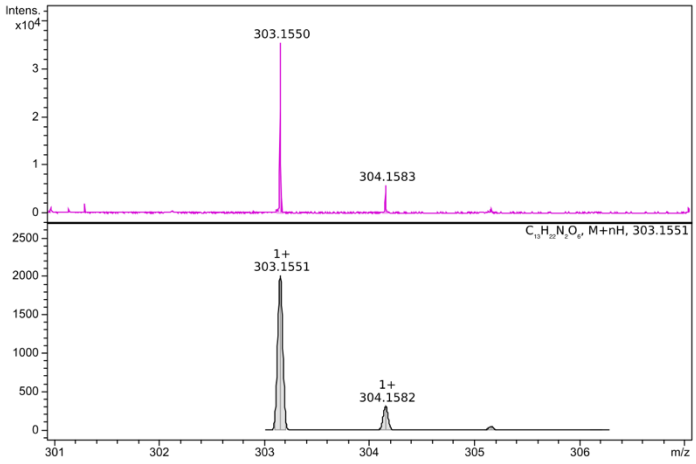

Figure S7. Comparison of the measured (pink) and simulated (black) $[M+H]^+$ mass spectra for palythinol.

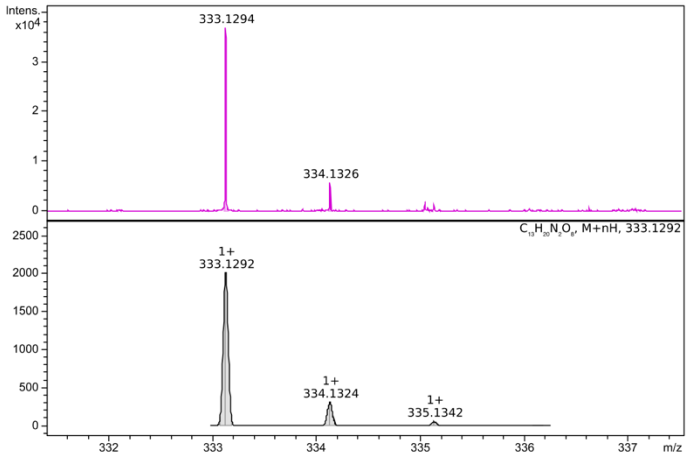

Figure S8. Comparison of the measured (pink) and simulated (black) $[M+H]^+$ mass spectra for shinorine.

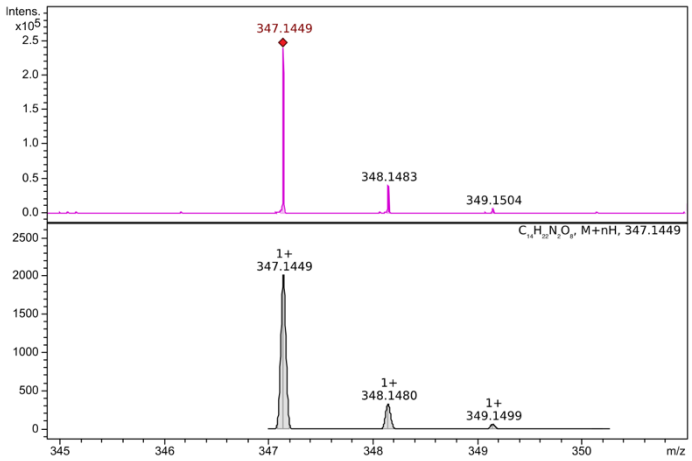

Figure S9. Comparison of the measured (pink) and simulated (black) $[M+H]^+$ mass spectra for porphyra-334.

Isolation of MAAs

Reverse-phase HPLC was performed using a PrepHT XDB-C18 column (21.2 mm × 100 mm, particle size 5 µm) connected to a 1260 HPLC equipped with a binary pump and diode-array detector (Agilent Technologies). Injection volumes of 200 µL were used with the following conditions: an isocratic hold of 5% B for 15 min increasing to 10% B for 10 min; then increasing to 100% B over 5 min; and finally, 100% B for 10 min (solvent A = 0.1% formic acid in water; solvent B = 0.1% formic acid in methanol) with a flow rate of 5 mL/min. The fractions absorbing at 320 nm and 334 nm were collected using an automated fraction collector and dried using a centrifugal evaporator afterwards. The dominant MAA in the 320 nm fraction was palythine and the dominant MAA in the 334 nm fraction was porphyra334. We make this conclusion based off the peak absorptions of each MAA in addition to the UHPLCHRMS analysis given above. Details including purification and experimental results regarding usujirene and palythene have been previously reported.[4]

Steady-state spectroscopy

UV-visible spectra were acquired using a UV-visible spectrometer (Cary 60, Agilent Technologies). For solution-phase experiments, samples were contained in a 1 cm pathlength quartz cuvette. For UVvisible spectra acquired on the model skin (Vitro Corneum), the skin was placed on a 2 mm CaF_2 window and mounted into a mirror mount before placed in the beam path of the UV-visible spectrometer.

The long-term photostability of the solution-phase samples were investigated by irradiation with a solar simulator (LSC-100 model 94011A, Oriel Instruments). The power experienced by the sample was 1000 W m^{-2} which is equivalent to the power of the sun at the Earth's surface and the solar simulated spectrum is given in Figure S10. Over a two hour irradiation period, the samples were continuously stirred and UV-visible spectra were recorded at regular intervals. The Area Under the Curve Index (AUCI) was determined following Equation 1:

$$AUCI = \frac{AUC_{after}}{AUC_{before}} \quad (1)$$

where AUC_{after} is the area under the curve between 280 and 400 nm after irradiation and AUC_{before} is the area under the curve between 280 and 400nm before irradiation.

Fluorescence spectra were obtained using a spectrofluorometer (Fluorolog 3, Horiba) set up with an emission and excitation bandwidth of 2.5 nm and an excitation wavelength corresponding the peak absorption of each sample.

Transient electronic absorption spectroscopy (TEAS)

The femtosecond TEAS setup used to monitor the photodynamics of the crude extract and purified MAAs has been previously described,[5] however, a brief outline and experimental details specific to the present work will be given here.

Solutions of crude extract in water and glycerol (MAA concentration ~150 μM) were circulated through a demountable liquid cell (Harrick Scientific Products Inc.) using a diaphragm pump (SIMDOS 02). The path length of the demountable liquid cell was 950 μm and was achieved by placing PTFE spacers between two CaF_2 windows (front window 2 mm and back window 2 mm thickness). Due to the smaller amount of samples of palythine and porphyra-334, aqueous solutions of ~40 μM were contained in a 1 mm pathlength quartz cuvette and continuously translated in the x and y direction. For the measurements on a skin mimic (Vitro Corneum), solutions of crude extract in glycerol and water were prepared (MAA concentration ~3 mM). The crude extract in glycerol sample was then applied, onto a piece of Vitro Corneum (~2 cm^2) which was on a 2 mm CaF_2 window, using a paintbrush to get even coverage and to remove any excess (referred to as skin I within this work). Approximately 0.2 mL of the crude extract in water sample was applied onto a piece of Vitro Corneum (~2 cm^2) which was on a 2 mm CaF_2 window and spread out evenly before leaving for at least an hour for the water to evaporate (referred to as skin II within this work). A higher concentration was used for the skin measurements to ensure the signal-to-noise was adequate for our experiments. For the skin measurements, the sample was moved for each scan to ensure that a new spot was irradiated each time.

The pump pulses for the TEAS experiment were generated using a tuneable optical parametric amplifier (TOPAS-C, Spectra-Physics) and was 320 nm for palythine in water, 334 nm for porphyra334 in water, 324 nm for crude extract in water, and 327 nm for crude extract in glycerol, skin I and skin II. The chosen wavelengths correspond to their peak absorption. The power of the pump pulse was set to 500 μW. The probe pulses for the TEAS experiment were generated by focussing a portion of the fundamental 800 nm beam onto a vertically translating CaF_2 window (2 mm thickness) to generate a white light continuum spanning 310-740 nm. A gold retroreflector mounted onto a motorised delay stage was used to vary the path length of the 800 nm beam that generates the probe pulse to give pump-probe time delays (Δt) between -1 and 1800 ps. Before reaching the sample, the pump beam passes through an optical chopper operating at a repetition rate of 500 Hz, blocking every other pulse of the 1 kHz pulse train. This enabled the pump-on and pump-off absorbance to be directly compared with a resultant output of difference in optical density (ΔOD). Two different setups on our table were used in this work; for the solution-phase experiments our standard setup (vertical setup) was used which is where the sample is mounted vertically, and for the skin experiments, the samples are mounted horizontally (horizontal setup). For the latter, the beam path of the pump and probe pulses are directed up towards the ceiling via periscopes before being directed back down towards the floor and through the sample. A full characterisation of this setup has been reported elsewhere.[6] The choice to mount the skin I and II samples horizontally was to ensure uniformity in the sample without any dripping off. As a result of the two different setups, the pump beam focus differs between the setups resulting in measured pump beam diameters at the sample of ~450 μm and ~350 μm for the vertical and horizontal setups respectively.

The TEAS data for porphyra-334 was acquired using the setup in the Warwick Centre for Ultrafast Spectroscopy (WCUS) due to setup availability. This setup has been described elsewhere,[7] but a difference to note is that the $\underline{\Delta t}$ extends out to 3000 ps.
The resultant transient absorption spectra (TAS) were chirp-corrected using the software package KOALA and the data was fit using a global sequential kinetic model $A \overset{\tau_1}{\rightarrow} B \overset{\tau_2}{\rightarrow} C$ ... using the software package Glotaran.[8,9]

Terahertz (THz) spectroscopy

The terahertz (THz) transmission spectroscopy was conducted with a Tera-K15 (MENLO Systems GmbH.) THz time-domain spectroscopy (THz-TDS) system. The system has a usable bandwidth in the frequency range of 0.1-5 THz and an acquisition rate of 4 Hz. In this study we analysed data ranging from 0.1-1 THz as higher frequencies are more strongly attenuated and sensitive to scattering effects. For the transmission measurements, the crude extract solution (~3 mM MAA concentration in glycerol) was contained in a liquid sample cell, which was formed with two 25mm quartz windows ($n\text{-} = 2.1 - 0.0001i$) separated by a 200 μm-thick Teflon spacer. The crude extract solution was measured before and after 2 hours of irradiation with a solar simulator (LSC-100 model 94011A, Oriel Instruments) with 50 pulses acquired each time (THz beam diameter = 5 mm).
The equipment described above was changed to reflection geometry, with the emitter and detector situated below a quartz imaging window and at a 30° incidence angle to the window. A pressure sensor was placed at either side of the top surface of the imaging window, where the subjects would place their volar forearms. This was to control the pressure during the measurements, to ensure sufficient pressure was applied for a good contact between the volar forearm and imaging window by avoiding the possibility of an air gap occurring. Additionally, the pressure was kept in the same range of 1.5-2.5 N cm^{-2} as to limit the effect of varying pressure on the skin measurements.[10] Data for three subjects were collected. Subjects arrived in the laboratory 15 minutes prior to their measurements, as this gave their skin time to acclimatise to the controlled room conditions of the laboratory. This was to control the effect of room temperature and humidity, known to affect the THz response of the skin.[11] Subjects remained in the laboratory for the duration of the experiment for the same purposes. Written informed consent was obtained from each subject prior to their involvement in the study. The study was approved by the Biomedical Scientific Research Ethics Committee, BSREC, (REGO-20182273 AM03).
The initial measurements of a single point scan consisting of approximately 280 pulses were measured on both volar forearms of each subject. 0.1 ml of Glycerol was applied to the 2.5 cm^2 measured region on the right arm of each subject, with the left arm left blank as a control. After 10 minutes had passed, both volar forearms were measured again, in the same location and using the same method as previously.

Experimental Results Details

Determination of MAA yield

The percentage dried weight was estimated by dissolving a known mass of crude extract in a known volume of water. A UV-visible spectrum was acquired of said sample by further dilution and the absorbance was used to work out an approximate MAA concentration using an average of the molar absorptivities of palythine and porphyra-334 (39250 M^{-1} cm^{-1}) and the Beer-Lambert law.[3] With a concentration and known volume, the mass of MAAs could be obtained. This is then calculated as a percentage dried weight based on the known mass of crude extract initially measured. We reiterate that the percentage dried weight we report is an approximate percentage dried weight.

Extended UV-visible spectrum of the crude extract

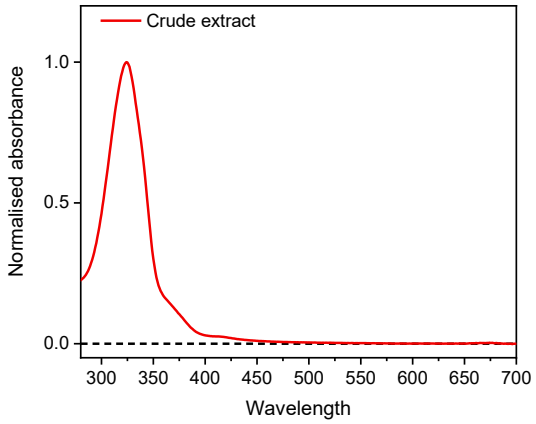

Figure S10. Normalised UV-visible spectrum from 280-700 nm of the crude extract in water.

Solar simulator spectrum

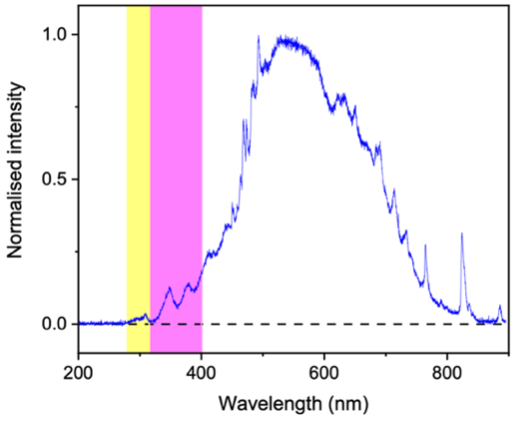

Figure S11. The spectrum output by the solar simulator used for the irradiation experiment in this work. Highlighted in pink is the UVA region (400-315 nm) and highlighted in yellow is the UVB region (315-280 nm).

Thickness of skin sample

The thickness of the film in skin I was determined by UV-visible spectroscopy. Five spectra were acquired and then averaged. The absorbance at the average peak absorption was then used to determine the pathlength using the Beer-Lambert law. Like before in determining the MAA yield, an average of the molar absorptivities of palythine and porphyra-334 (39250 M^{-1} cm^{-1}) was used.[3] We again acknowledge that we have made assumptions here, but it will give us a reasonable approximation of the thickness.

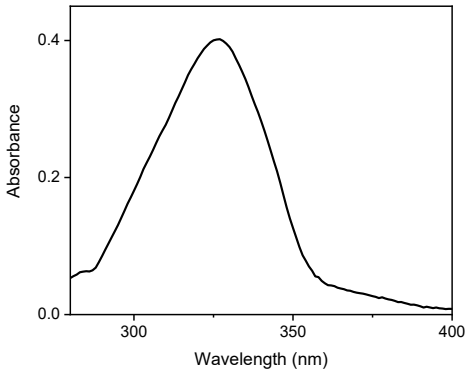

Figure S12. Averaged UV-visible spectrum of the skin I sample.

Transient electronic absorption spectroscopy in water

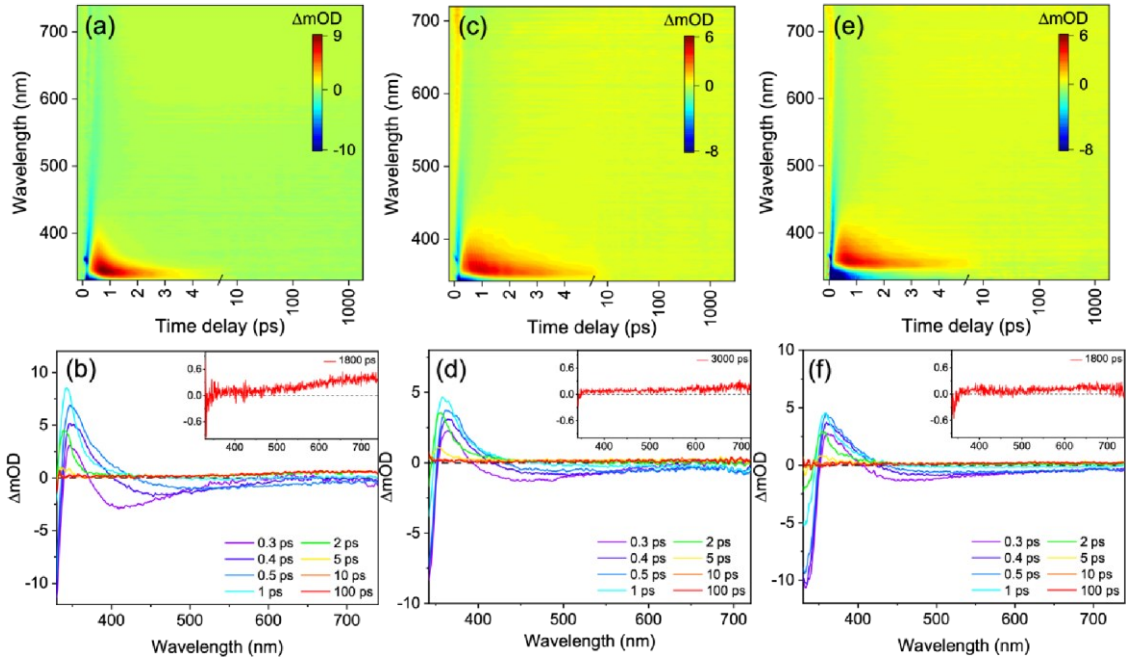

Figure S13. TAS of palythine in water presented as (a) false colour heat map and (b) lineouts, porphyra-334 in water presented as (c) false colour heat map and (d) lineouts, and crude extract in water presented as (e) false colour heat map and (f) lineouts. Time delays in (a), (c) and € are plotted linearly until 5 ps and then as a logarithmic scale from 5 to 1800 ps or 3000 ps. In (b), (d) and (f) the inset is of a high average transient at 1800 or 3000 ps.

Solvated electron test

Below presents TAS of palythine and the crude extract in water (black trace) and when in a potassium nitrate aqueous solution (red trace). In the presence of potassium nitrate (a known solvated electron scavenger),[12] the signal above ~500 nm disappears confirming that the signal corresponds to solvated electron.

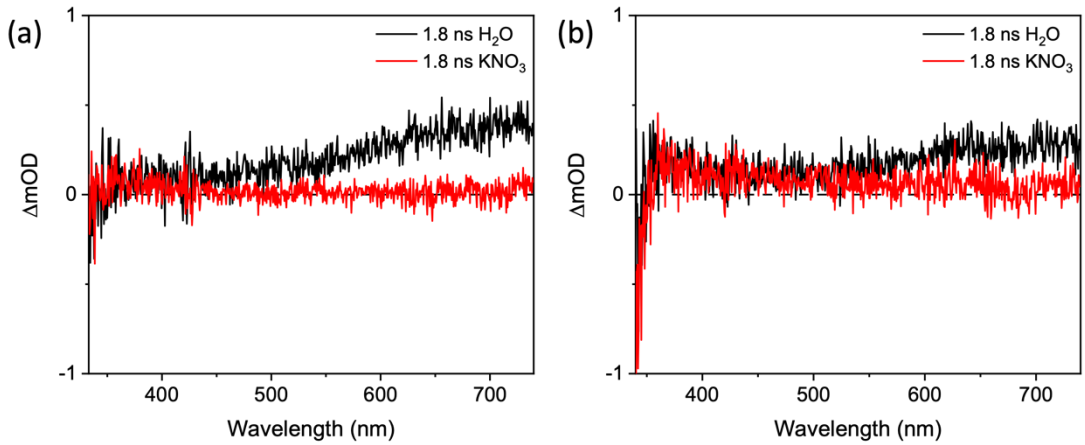

Figure S14. 1.8 ns TAS of (a) palythine and (b) crude extract in water (black trace) and in a potassium nitrate aqueous solution (red trace).

Fluorescence spectra

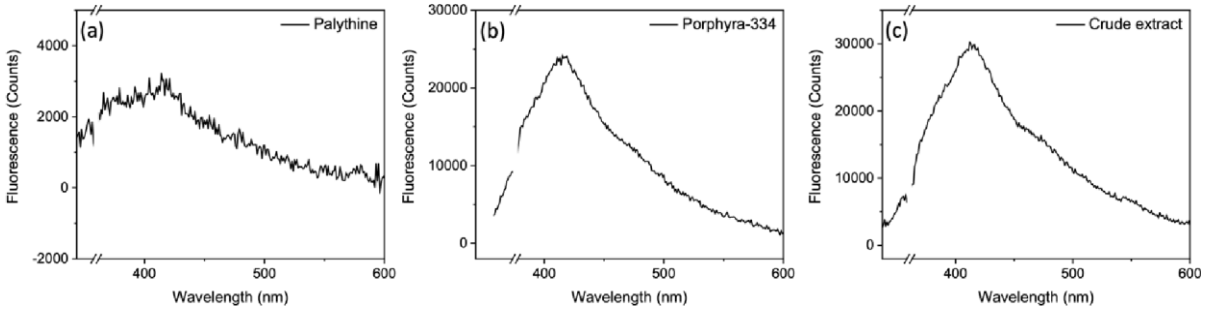

Figure S15. Fluorescence spectra of (a) palythine in water, (b) porphyra-334 in water and (c) crude extract in water.

Evolution associated difference spectra (EADS) and residuals

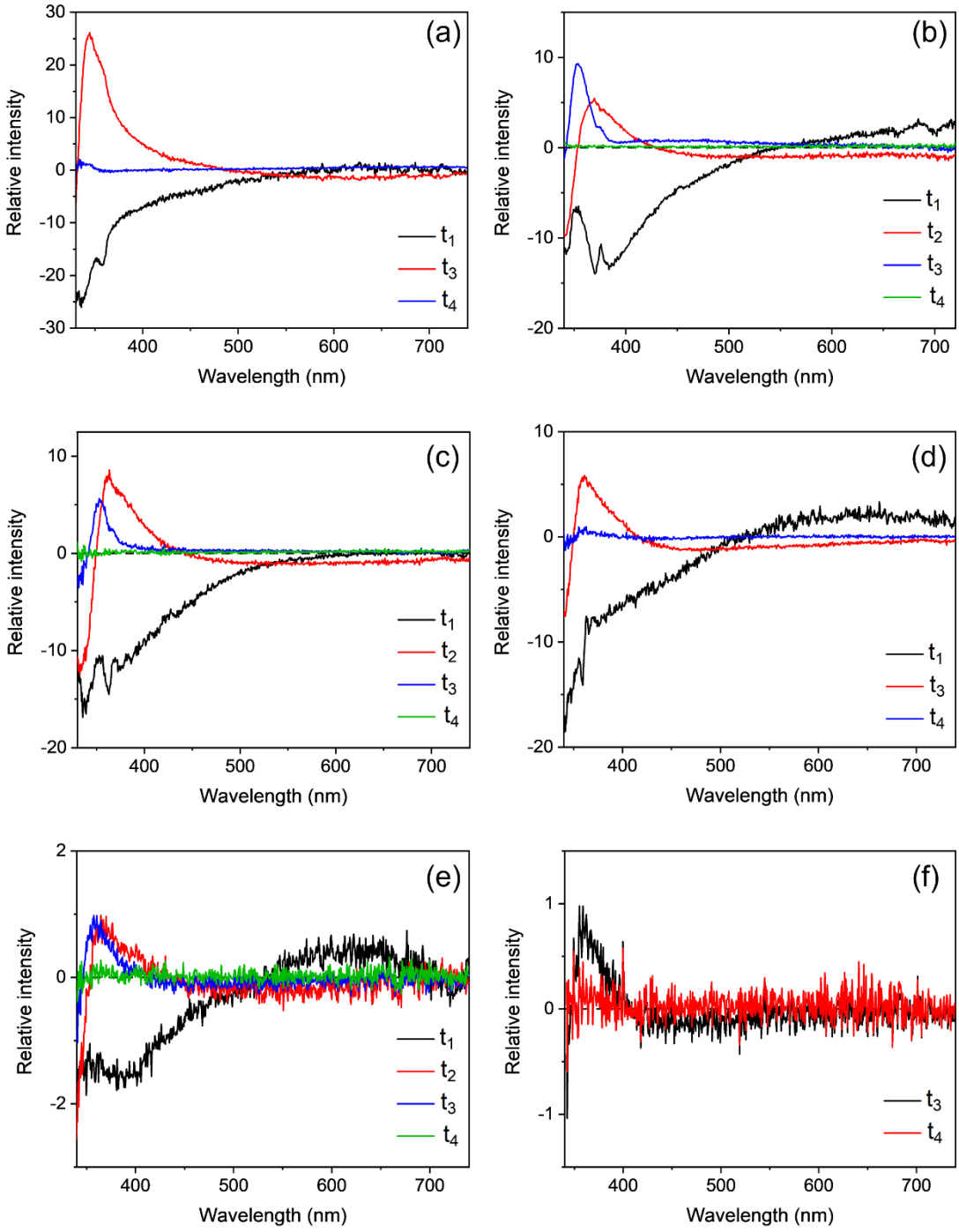

Figure S16. EADS for (a) palythine in water photoexcited at 320 nm, (b) porphyra-334 in water photoexcited at 334 nm, (c) crude extract in water photoexcited at 324 nm, (d) crude extract in glycerol photoexcited at 327 nm, (e) crude extract (skin I) photoexcited at 327 nm and (f) crude extract (skin II) photoexcited at 327 nm.

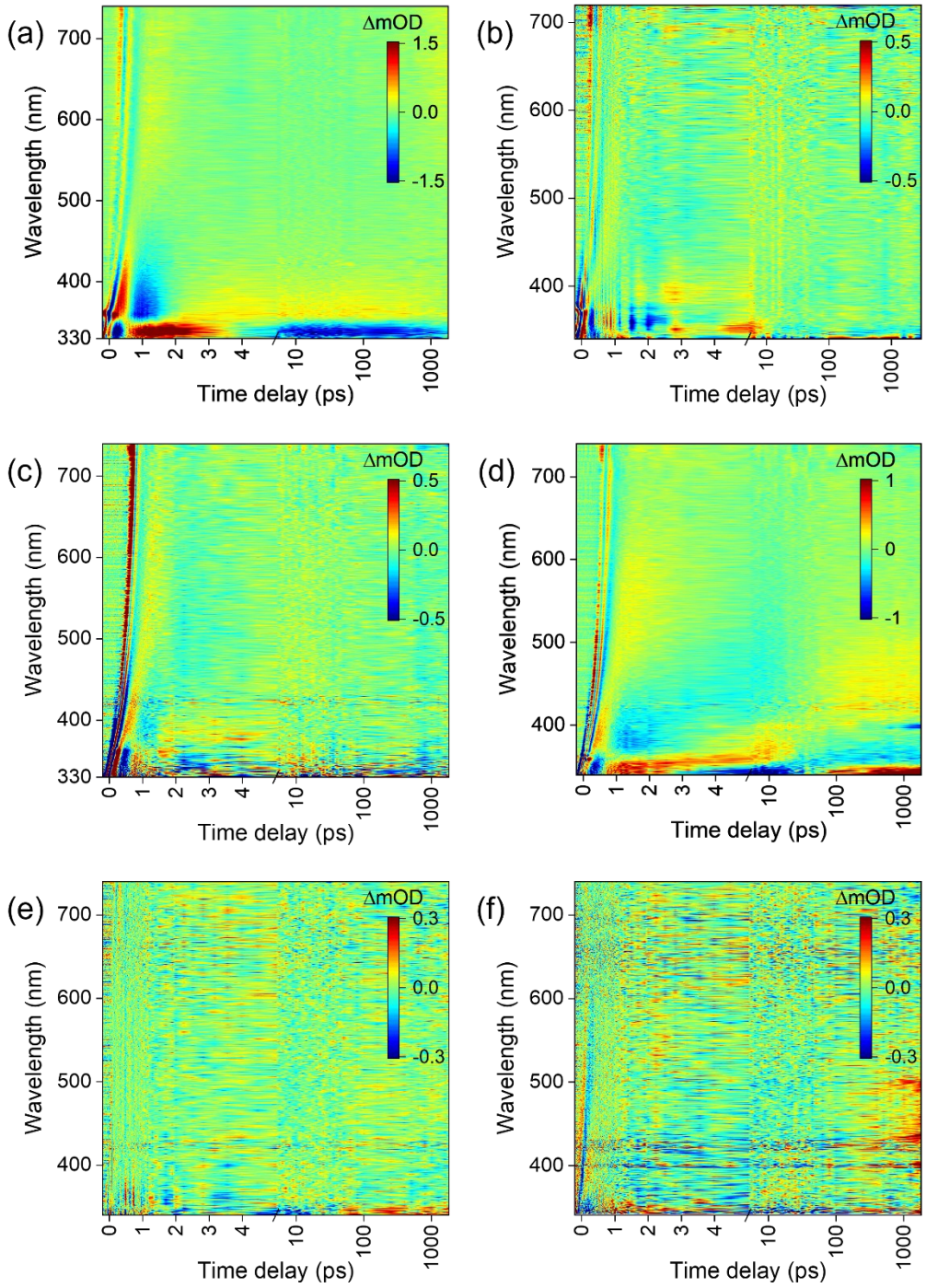

Figure S17. False colour heat maps of the fitting residuals for (a) palythine in water photoexcited at 320 nm, (b) porphyra-334 in water photoexcited at 334 nm, (c) crude extract in water photoexcited at 324 nm, (d) crude extract in glycerol photoexcited at 327 nm, (e) crude extract (skin I) photoexcited at 327 nm and (f) crude extract (skin II) photoexcited at 327 nm. Time delays are plotted linearly until 5 ps and then as a logarithmic scale from 5 to 1800 ps or 3000 ps in the case of (b). The fitting residuals have not been chirp corrected.

Instrument response function

The full width half maximum (FWHM) of our instrument response function provides an initial guess for one of the input parameters within Glotaran (which is subsequently allowed to iterate). In order to attain this initial guess, we conducted solvent-only transients. To this data, we fit a frequencydependent cross-correlation function (which takes into account any artefact contributions from the solvent and/or Harrick cell windows), $F_{cc}(w,t_d)$ given by Equation 2:[13]

$$F_{cc} \approx \exp\left\{-\frac{\left[t_d+(t_0(\omega))^2\right]}{\tau^2}\right\} \quad (2)$$

Here, t_d is pump-probe time delay, $t_0(w)$ is the temporal overlap between the pump and probe (for a given w) and t is the pump pulse duration which is 70 fs for both water and glycerol. The chosen wavelength region was an average signal between 388-390 nm as this is a wavelength region where we observe notable dynamics. The quoted errors in Table 2 are half of the FWHM of the instrument response function if the error output by the fitting software is smaller than that.

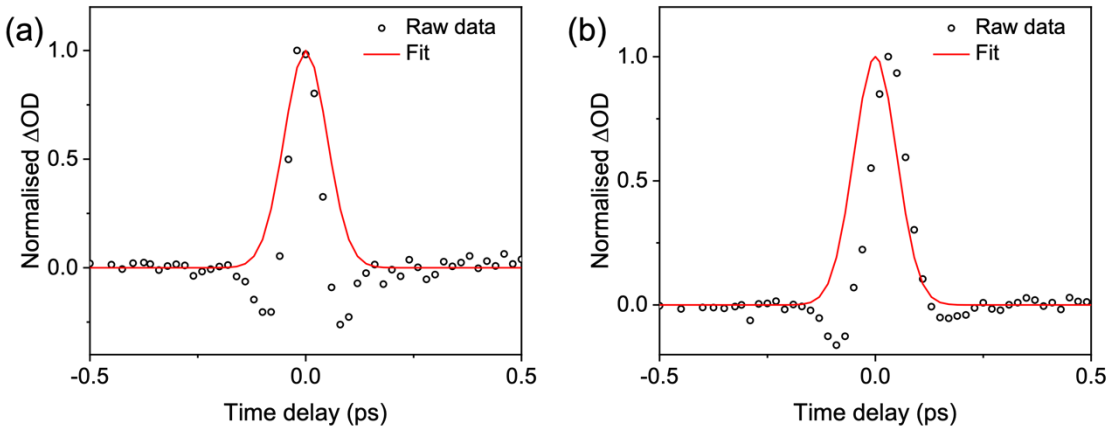

Figure S18. Transient at 388-390 nm for solvent-only time-zero response of (a) water photoexcited at 333 nm (open back circles) and (b) glycerol photoexcited at 327 nm (open black circles). The pump probe cross-correlation (F_{CC}) is overlaid (red line) and the returned FWHM of the F_{CC} is ~120 fs in both cases which corresponds to the FWHM of the instrument response function.

References

1. Y. V. Yuan, N. D. Westcott, C. Hu and D. D. Kitts, Food Chem., 2009, 112, 321-328.
2. Y. Nishida, Y. Kumagai, S. Michiba, H. Yasui and H. Kishimura, Mar. Drugs, 2020, 18, 502.
3. V. Geraldes and E. Pinto, Pharmaceuticals, 2021, 14, 63.
4. A. L. Whittock, J. M. Woolley, N. Auckloo, C. Corre and V. G. Stavros, Molecules, 2022, 27, 2272.
5. S. E. Greenough, G. M. Roberts, N. A. Smith, M. D. Horbury, R. G. McKinlay, J. M. Żurek, M. J. Paterson, P. J. Sadler and V. G. Stavros, Phys. Chem. Chem. Phys., 2014, 16, 1914119155.
6. T. T. Abiola, B. Rioux, S. Johal, M. M. Mention, F. Brunissen, J. M. Woolley, F. Allais and V. G. Stavros, J. Phys. Chem. A, 2022, 126, 8388-8397.
7. J. M. Woolley, M. Staniforth, M. D. Horbury, G. W. Richings, M. Wills and V. G. Stavros, J. Phys. Chem. Lett., 2018, 9, 3043-3048.
8. M. P. Grubb, A. J. Orr-Ewing and M. N. R. Ashfold, Rev. Sci. Instrum., 2014, 85, 064104.
9. J. J. Snellenburg, S. Laptenok, R. Seger, K. M. Mullen and I. H. M. Van Stokkum, J. Stat. Softw., 2012, 49, 1-22.
10. J. Wang, R. I. Stantchev, Q. Sun, T. W. Chiu, A. T. Ahuja and E. P. MacPherson, Biomed. Opt. Express, 2018, 9, 6467-6476.
11. H. Lindley-Hatcher, A. I. Hernandez-Serrano, Q. Sun, J. Wang, J. Cebrian, L. Blasco and E. Pickwell-MacPherson, J. Infrared Millim. Terahertz Waves, 2019, 40, 980-989.
12. X. Chen, D. S. Larsen, S. E. Bradforth and I. H. M. van Stokkum, J. Phys. Chem. A, 2011, 115, 3807-3819.
13. S. A. Kovalenko, A. L. Dobryakov, J. Ruthmann and N. P. Ernsting, Phys. Rev. A, 1999, 59, 2369-2384.